

Simulation of earing during deep drawing of an Al–3% Mg alloy (AA 5754) using a texture component crystal plasticity FEM

I. Tikhovskiy, D. Raabe*, F. Roters

Max-Planck-Institut für Eisenforschung, Department Microstructure Physics and Metal Forming, Max-Planck-Straße 1, D-40237 Düsseldorf, Germany

Received 20 December 2005; received in revised form 4 October 2006; accepted 5 October 2006

Abstract

A texture component crystal plasticity finite element method (TCCP-FEM) is used for the simulation of the deep drawing process of sheet aluminium of the alloy AA 5754 (AlMg₃, 3.3535). The method incorporates the texture of the starting material and predicts the earing behaviour during cup drawing considering the 12 {1 1 1}⟨1 $\bar{1}$ 0⟩ slip systems. The results are compared to experimental data and to yield surface simulations. © 2006 Elsevier B.V. All rights reserved.

Keywords: Texture; Anisotropy; Crystal plasticity; Finite element simulation; Yield surface; Earing; Deep drawing; Sheet forming; FCC; Aluminium alloy

1. Introduction

Engineering polycrystalline materials often exhibit significant elastic–plastic anisotropy that can be attributed to the presence of crystallographic texture. In the early industrial practice texture was long a property of polycrystals which was simply inherited from the preceding processing steps without conducting particular anisotropy optimization. This means that textures were known as an inevitable side-effect of materials processing which was hard to avoid and often accepted as it was. In contrast, modern industrial process design gradually aims at optimizing microstructures and properties during production, i.e. its goal consists in exploiting metallurgical mechanisms such as crystal plasticity, recrystallization, grain growth, and phase transformation for the design of well tailored crystallographic textures with respect to certain desired anisotropy properties of the final product.

The most recent phase in the advancement of quantitative texture and anisotropy engineering consists in the introduction of inverse texture simulation methods. Such approaches are designed for the physically based tailoring of optimum textures for final products under consideration of prescribed processing and materials conditions on an inverse basis. This means that variational texture optimization can nowadays be conducted in

a way to match some desired final anisotropy and can help to identify beneficial corresponding processing parameters. This amounts to a tenet change in the sense that the process should no longer determine the textures but the desired textures should determine the process.

Plastic anisotropy during deep drawing may entail the formation of uneven rims of the drawn product, usually referred to as *earing*. One important consequence of that is – besides the irregular shape of the drawn specimen – an inhomogeneous distribution of the mechanical properties and of the wall thickness due to volume conservation and the kinematically necessary strain rate variation.

The aim of this study, therefore, lies in an improved prediction of earing during deep drawing of sheet aluminium alloy (AlMg₃) using the texture component crystal plasticity finite element method (TCCP-FEM) with 12 slip systems. This method works by using spherical orientation components for the texture approximation instead of sets of single orientations. More details on this approach are given in the ensuing section and in [1–10]. The measured texture of a rolled aluminium alloy sheet, fitted by using the texture component method, was used as the starting texture for the FE calculation. The resulting earing profiles are compared with results obtained by use of Hill's 1948 yield surface as well as with experimental data. As the texture component crystal plasticity finite element method is based on crystal plasticity it not only accounts correctly for the anisotropy due to the starting texture of the material, it also includes the change of anisotropy due to texture evolution

* Corresponding author. Tel.: +49 211 6792278; fax: +49 211 6792333.
E-mail address: raabe@mpie.de (D. Raabe).

during the forming operation. In contrast, the Hill-based yield surface simulation does not update the texture during forming.

2. The texture component crystal plasticity finite element method

A challenge of integrating constitutive polycrystal plasticity laws into finite element approaches lies in identifying an efficient method of mapping a crystallographic texture which represents a large number of grains on the integration points of a finite element mesh. Such an approach must be formulated in a way that still permits texture update in the course of the forming simulation. It is an important condition in that context that crystal plasticity finite element models require a *discrete* representation of the orientation distribution function (ODF) at each integration point. For relatively small numbers of grains (less than 10^3 crystals) the discrete mapping of the texture on the mesh can be achieved by a one-to-one approach, where each integration point in the finite element grid is characterized by one crystallographic orientation. For large assemblies of grains this approach does no longer work.

The main task of the texture component crystal plasticity finite element concept is to represent sets of spherical Gaussian texture components [11–14] on the integration points of a finite element mesh for a crystal plasticity simulation. This procedure works in two steps: first, for each texture component selected its discrete *center* orientation is assigned in terms of its respective Euler triple $(\varphi_1, \Phi, \varphi_2)$, i.e. in the form of a single rotation matrix, onto each integration point. In the second step, this discrete central orientation of each of the mapped Gauss distributions is systematically on each integration point re-oriented in such a fashion that the resulting overall distribution reproduces the texture function which was originally prescribed. After this mapping procedure the texture simulation is conducted in the form of a conventional crystal plasticity finite element model according to the approach of Kalidindi et al. [15]. Details of the texture component crystal plasticity finite element approach are given in [1–10].

3. Yield surface

Various concepts exist to solve the problems of mapping texture-related sheet anisotropy into finite element models for sheet forming. Incorporation of the initial material anisotropy existing before sheet deformation into the finite element codes can be realized either through an anisotropic yield surface function or directly via crystallographic texture models.

One of the groups of the anisotropic yield surface models comprises empirical and phenomenological anisotropic yield surface equations, such as the equations of Hill from 1948 [16] and 1979 [17], Hosford [18], Barlat [19], or Barlat and Lian [20], to name but a few important ones. These yield surface functions are formulated as convex higher-order polynomials, i.e. they take an empirical view at plastic anisotropy. The physical nature of anisotropy can be incorporated into these concepts, for instance, by fitting the corresponding polynomial coefficients with the aid of texture-based strain rate or self-consistent homogenization

methods or with anisotropy parameters obtained from mechanical tests.

Hill's 1948 classic yield surface function is the most prominent and frequently used yield function to account for plastic anisotropy, mainly due to its simple handling in manual as well as in numerical calculations. Hill's 1948 potential function is a simple extension of the isotropic von Mises function, which can be expressed in terms of rectangular Cartesian stress components as:

$$f(\sigma) = (F(\sigma_{22} - \sigma_{33})^2 + G(\sigma_{33} - \sigma_{11})^2 + H(\sigma_{11} - \sigma_{22})^2 + 2L\sigma_{23}^2 + 2M\sigma_{31}^2 + 2N\sigma_{12}^2)^{1/2} \quad (1)$$

where 1, 2, and 3 usually represent in the case of sheet materials the rolling direction (RD), transverse direction (TD) and normal direction (ND), respectively. F , G , H , L , M and N are constants obtained by material tests in different orientations. They are defined as functions of the uniaxial yield stresses:

$$\begin{aligned} F &= \frac{1}{2R_{22}^2} + \frac{1}{2R_{33}^2} - \frac{1}{2R_{11}^2}, & G &= \frac{1}{2R_{11}^2} + \frac{1}{2R_{33}^2} - \frac{1}{2R_{22}^2}, \\ H &= \frac{1}{2R_{11}^2} + \frac{1}{2R_{22}^2} - \frac{1}{2R_{33}^2}, & L &= \frac{3}{2R_{23}^2}, \\ M &= \frac{3}{2R_{13}^2}, & N &= \frac{3}{2R_{12}^2} \end{aligned} \quad (2)$$

where R_{ij} are ratios of measured yield stress to the reference yield stress. In MARC one has to specify up to six of these values. For general planar anisotropy only four yield stress ratios are needed, which can be calculated from the r -value for the angles 0° , 45° and 90° with respect to the rolling direction of the sheet. The r -value is the ratio of the strain components ε_{33} and ε_{22} and is usually experimentally determined at a technical tensile strain of 20%.

The main advantages of empirical anisotropic yield surface functions as constitutive laws in metal forming finite element simulations are short calculation times and (for special cases with stable textures) robust results. The main disadvantage lies in the fact that the anisotropy of metals do not consider that the inherited sheet starting textures may evolve further in the course of sheet forming. For details of the implementation in FEM-Programs see [21,22].

4. Presentation of texture components of face centered cubic (FCC) metals

Owing to the cubic symmetry of the face centered cubic crystal system and the orthorhombic sample system which is set up by the rolling direction, normal direction, and transverse direction of the sample, textures of rolled FCC polycrystals are typically presented in the reduced Euler space where an orientation is given by the three Euler angles φ_1 , Φ and φ_2 , ($0^\circ \leq \varphi_1, \Phi, \varphi_2 \leq 90^\circ$). The Bunge notation is used for the Euler angles throughout this article [23]. Crystal orientations can also be conventionally describes by the use of Miller indices $\{hkl\}\langle uvw\rangle$. In this concept the triple $\{hkl\}$ describes the crystallographic

plane parallel to the sheet surface whereas $\langle uvw \rangle$ indicates the crystal direction parallel to RD.

Important texture components are on the α_{fcc} -fiber which comprises all orientations with a common crystallographic fiber axis $\langle 011 \rangle$ parallel to ND including major components $\{011\}\langle 100 \rangle$ (Goss-component, $\varphi_1 = 0^\circ$, $\phi = 45^\circ$, $\varphi_2 = 0^\circ$), $\{011\}\langle 211 \rangle$ (brass-component, $\varphi_1 = 35^\circ$, $\phi = 45^\circ$, $\varphi_2 = 0^\circ$), $\{011\}\langle 111 \rangle$, and $\{011\}\langle 011 \rangle$ (90° about the normal rotated Goss-component, $\varphi_1 = 90^\circ$, $\phi = 45^\circ$, $\varphi_2 = 0^\circ$) and the less symmetric β -skeleton line including major components $\{211\}\langle 111 \rangle$ (copper-component, $\varphi_1 = 90^\circ$, $\phi = 35^\circ$, $\varphi_2 = 45^\circ$), $\{123\}\langle 634 \rangle$ (S-component, $\varphi_1 = 60^\circ$, $\phi = 32^\circ$, $\varphi_2 = 65^\circ$), and the brass component $\{011\}\langle 211 \rangle$ ($\varphi_1 = 35^\circ$, $\phi = 45^\circ$, $\varphi_2 = 0^\circ$) [24–27].

The rolling texture in aluminium alloys is primarily composed of the S orientation, $\{123\}\langle 634 \rangle$, the brass orientation, $\{110\}\langle 1\bar{1}2 \rangle$, and the copper orientation $\{112\}\langle 11\bar{1} \rangle$. These texture components promote earing essentially at $45^\circ/135^\circ$ with respect to the rolling direction. Annealing textures which may contain the cube orientation, $\{100\}\langle 001 \rangle$, and also some Goss orientation, $\{110\}\langle 001 \rangle$, also promote pronounced earing, namely, at the $0^\circ/90^\circ$ directions for the cube orientation and the Goss orientation [28–36]. A useful approach, therefore, might consist in creating a sheet material with a low ear ratio by a suitable combination of crystals with an orientation that results in $45^\circ/135^\circ$ ears and those that produce $0^\circ/90^\circ$ ears [28,29].

5. Experimental procedures

5.1. Material, texture and metallography

The material used in this study was aluminium alloy sheet AlMg₃ (AA 5754/3.3535) with an initial thickness of 1.45 mm. The chemical composition is given in Table 1. Since the texture of aluminium alloys is often inhomogeneous through the thickness [37–39], the crystallographic texture of the starting sheet was investigated at the surface and in the center layers. Parameter $s = a(0.5d)^{-1}$ is defined to describe the actual layer position, where a is the distance between the actual layer inspected and the sample center layer, and d the thickness of

the sheet, i.e. the surface layer is defined by $s = 1$ and the center layer by $s = 0$. To remove a surface layer of 10–15 μm for texture measurements, the samples were etched in a solution of 20 mL H₂O, 20 mL HCl, 20 mL HNO₃ and 5 mL HF at room temperature.

The textures were investigated quantitatively by measuring the three incomplete pole figures $\{111\}$, $\{200\}$ and $\{220\}$ from an area of 25 mm \times 25 mm in the range of the pole distance angle α from 5° to 85° using Cu K α 1 radiation in the back reflection mode. From the experimental pole figures the orientation distribution function, $f(g)$, was computed according to the method of series expansion ($l_{\text{max}} = 22$) with spherical harmonic functions [40]. Additionally, the experimentally obtained textures were fitted by the texture components method using the approach of Helming et al. [41].

Fig. 1 shows the microstructure of the aluminium alloy AlMg₃ in flat sections in the surface ($s = 1.0$) and center layers ($s = 0.0$). No substantial difference was found between the grain dimensions of the inspected layers. It must be noted, too, that in contrast to the center layer, bigger light areas are to be observed on the surface layer, which indicate non-recrystallized structure. Light microscopy reveals an average grain size of 22.1 μm (ASTM 8). Vickers hardness testing was conducted using a load of 98.0665N leading to HV10 hardness numbers. The average hardness amounted to 85.1 ± 0.62 HV10 on the surface and 83.6 ± 0.79 HV10 in the center layer. The mechanical and anisotropy properties were determined by tensile tests at 0° , 45° , and 90° relative to rolling direction (Table 2).

5.2. Set-up of the finite element model and simulation details

The texture component crystal plasticity finite element calculations were conducted by using MSC/MARC in conjunction with the user defined material subroutine HYPELA2 [5–7,42]. Due to the orthotropic sample symmetry, only a quarter of the blank was represented in the simulations. As the aluminium alloy AlMg₃ is a material with FCC lattice structure, the 12 $\{111\}\langle 1\bar{1}0 \rangle$ slip systems were used for the simulations.

As outlined in previous simulation studies the particular advantage of the crystal plasticity finite element approach lies in the fact that the required material input parameters have to be fitted only once by using corresponding single crystal flow curves or polycrystal flow curves (which have to be divided by the Taylor factor) [6,7,43–47]. Like in those previous works $\dot{\gamma}_0 = 0.001 \text{ s}^{-1}$ was used as reference value for the slip rate and the strain rate sensitivity parameter m is taken as 0.02. The hardening matrix parameters are $q^{\alpha\beta} = 1.0$ for coplanar slip and $q^{\alpha\beta} = 1.4$ for non-coplanar slip. The components of the elasticity tensor were taken as $C_{11} = 106.75$ GPa, $C_{12} = 60.41$ GPa, and $C_{44} = 28.34$ GPa. The values of the slip system hardening parameters h_0 , a and s_s , and the initial value of the slip resistance s_0 were taken to be $h_0 = 60$ MPa, $s_s = 75$ MPa, $a = 2.25$, and $s_0 = 12.5$ MPa.

Table 1
Nominal chemical composition of AlMg₃ in weight-%

Al	Mg	Mn	Fe	Cr	Cu	Ti	Zn	Si
Base	2.6–3.6	< 0.5	< 0.4	< 0.30	< 0.10	< 0.15	< 0.20	< 0.4

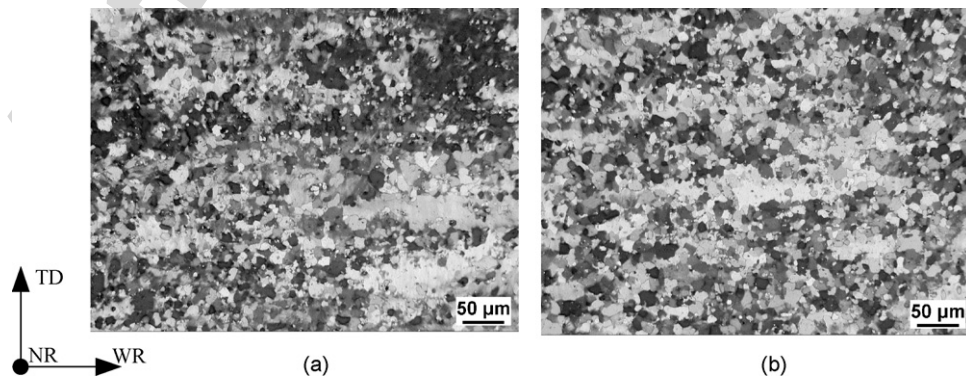


Fig. 1. Microstructure of the aluminium alloy AlMg₃ in flat sections: (a) surface layer ($s = 1.0$); (b) center layer ($s = 0.0$).

Table 2
Mechanical and anisotropic properties of AlMg₃

Angular offset from rolling direction (°)	Yield strength in MPa	Tensile stress in MPa	Elongation to fracture in %
0	157.3	233.2	15.5
45	155.4	223.8	18.9
90	152.4	221.7	19.5

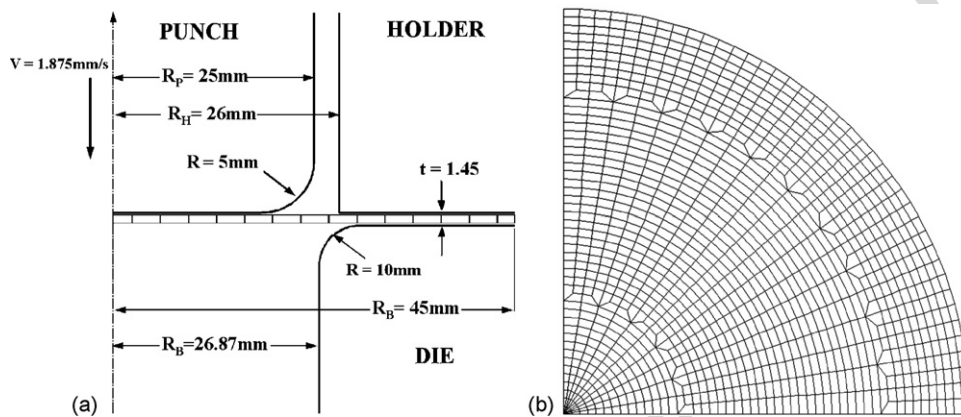


Fig. 2. (a) Finite element model showing the geometry of the tools in units of millimeter. (b) Mesh configuration.

Fig. 2a shows the geometry of the tools used in the simulation. Fig. 2b shows the mesh configuration of the specimen prior to loading. The angular element density increases from the blank center to the border in order to obtain good accuracy along the final border of the cup. The blank was modeled using 432 elements of type C3D8 and 80 elements of type C3D6. Fig. 2b shows the mesh configuration of the specimen. The Coulomb friction coefficient was assumed to be $\mu = 0.2$ between the punch and the blank. As also reported in earlier works [6,7,10] changes in the friction properties between $\mu = 0.1$ and 0.2 were systematically checked and the results showed that the friction coefficient had under these boundary conditions a relatively small influence on the relative ear height and on the earing shape.

5.3. Measurement of the ear profile

Measurement of the ear profile was performed with a self-built device. The cup-drawn aluminium sample fixed to the step motor was turned about 1.8° per step. After that the sensor automatically measured the change in the height of the ear. The program used for controlling the step motor, for measuring the ear height and for automatic data acquisition was written with the VEE Pro 6 (Hewlett-Packard Company, Englewood, USA) graphical programming environment.

6. Results and discussion

It is known that for the prediction of deformation textures the correct incorporation of the starting texture is important. The comparison of the recalculated $\{111\}$ and $\{200\}$ pole figures obtained from the texture component method with those which were experimentally determined for the surface and center layers are shown in Fig. 3. Besides the random texture portion seven components have to be used to approximate the experimental textures (Table 3). The recalculated textures show good agreement with the experimental pole figures although the overall pole density is somewhat weaker for the recalculated $\{111\}$ pole figures. The reason for this drop in the recalculated $\{111\}$ pole density might be that the texture component method has

limited possibilities in the uniqueness of the approximation of minor portions of the experimental texture data.

Moreover, due to insignificant differences between the original experimental textures at the center ($s = 0.0$) and surface layers ($s = 1.0$), the band reveals only a slight through-thickness texture gradient (Fig. 3). Owing to this fact, the initial texture of the aluminium alloy sheet was assumed to be homogeneous throughout the thickness. In this work, two earing calculations were performed using texture component crystal plasticity finite element method. In the first simulation, the texture components fitted from the center layer ($s = 0.0$), and in the second simulation the texture components fitted from the surface layer ($s = 1.0$) were mapped in the FE-model.

Fig. 4 shows the simulated and experimentally observed development of plastic earing in a cup-drawn aluminium alloy sample. It can be seen that the ear profiles generated by texture components fitted from the center layer ($s = 0.0$) and by texture components fitted from the surface layer ($s = 1.0$) are almost identical. The probable reason for it is that the texture components fitted from each layer (Table 3) of the aluminium alloy sheet reproduce nearly identical initial textures (Fig. 3), which were used further in TCCP-FE calculations.

The results (Fig. 4) show that the texture component finite element simulation fits the experimental results distinctly better than that obtained by help of the Hill yield surface. The major discrepancy between the Hill-based simulation and the experiment is that the Hill approach does not correctly predict the angular position of the maximum absolute earing height. The Hill-based simulation displaces the maximum by about 45° . The texture component method yields a good result for the position of the earing maximum and also shows good agreement for the shape of the earing curve particularly for small angles. The small height offset over the entire experimental earing profile can be

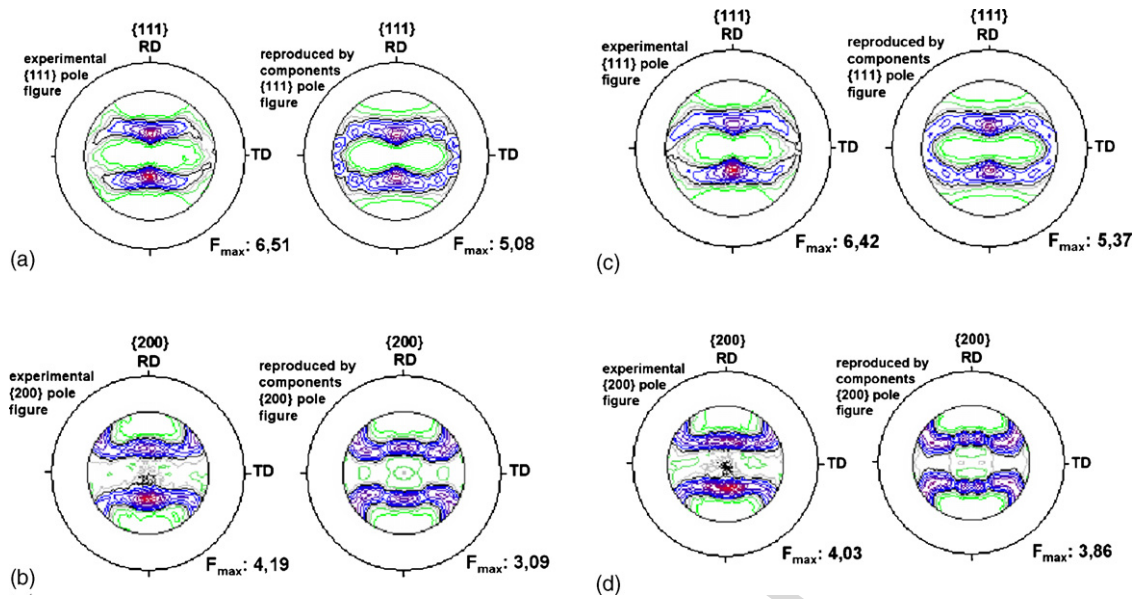


Fig. 3. The experimental and recalculated pole figure: (a and b) surface layer ($s=1.0$); (c and d) center layer ($s=0.0$).

attributed to insufficient approximation of the experimentally observed textures by the texture component approximation. This is evident from the fitted texture components listed in Table 3 and the corresponding comparison of the experimental and the recalculated pole figures in Fig. 3. This problem associated with the texture component approximation of the ODF lies in the fact that with decreasing intensity in the pole figures or, respectively, in the difference pole figures some ambiguity enters the approximation procedure as to what texture component really improves the texture fit. An improved decomposition method to extract single orientations from an ODF and map those onto the integration points of a FE mesh might render the texture fit procedure more robust and less ambiguous when it comes to small orientation densities.

Fig. 5 shows the resulting distribution of the relative wall thickness for the drawn cup simulated by the TCCP-FEM for texture components of the center layer ($s=0.0$). Similar results were obtained by the same simulation performed using the texture components of the surface layer as starting texture. As the texture component crystal plasticity finite element method uses volume elements for the FE simulation, the calculations

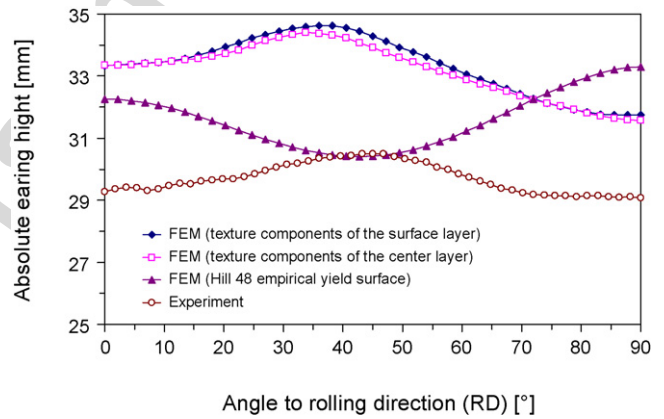


Fig. 4. Simulations and experiment of earing during cup drawing of aluminium alloy AlMg₃. The figure compares the texture component finite element simulation (TCCP-FEM) for texture components of the center ($s=0.0$) and surface ($s=1.0$) layers with a simulation obtained by use of a Hill 1948 yield surface using experimental r -values.

Table 3
Texture components used for the model approximation

Surface layer ($s=1.0$)						Center layer ($s=0.0$)					
	φ_1 [°]	Φ [°]	φ_2 [°]	b	V [%]		φ_1 [°]	Φ [°]	φ_2 [°]	b	V [%]
Comp. 1	41.4	38.3	80.6	16.7	33.16	Comp. 1	295.2	94.3	129.7	14.7	29.56
Comp. 2	133.3	71.6	64.3	13.4	22.88	Comp. 2	32.8	64.3	19.0	12.1	15.88
Comp. 3	324.0	62.2	73.2	17.0	10.04	Comp. 3	337.1	58.4	75.9	12.1	11.72
Comp. 4	168.5	40.3	91.0	13.8	7.96	Comp. 4	318.7	107.6	114.3	13.7	10.20
Comp. 5	240.6	71.1	110.2	19.1	6.84	Comp. 5	262.2	88.5	33.9	16.7	8.60
Comp. 6	260.6	82.5	24.5	16.1	5.44	Comp. 6	227.6	64.3	114.4	15.3	3.80
Comp. 7	180.2	86.3	91.7	15.5	3.44	Comp. 7	270.4	88.9	88.1	15.2	2.64
Random	10.24					Random	15.0				

$\varphi_1, \Phi, \varphi_2$: Bunge-Euler angles; V : volume fraction; scatter width: b .

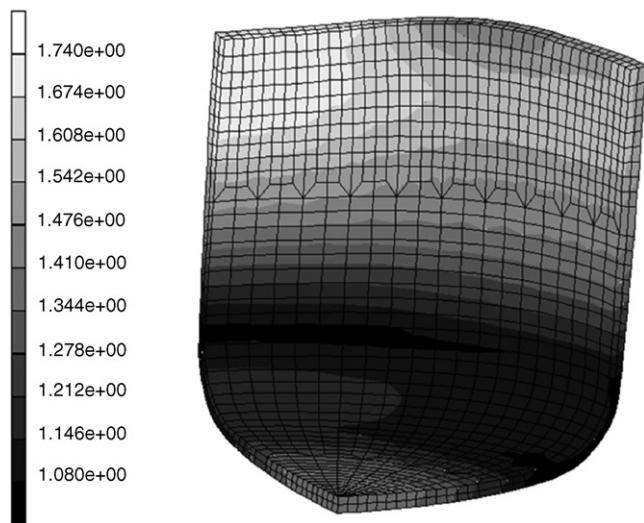


Fig. 5. Relative wall thickness of the drawn cup (darker is thinner) simulated by the texture component crystal plasticity finite element method (TCCP-FEM) for texture components of the center layer ($s=0.0$).

are not restricted to the plain strain case. The calculation of the sheet thickness becomes rather complicated in this general case. On the other hand, one may assume that the deformation state is very close to the plain strain situation which is typical of deep drawing operations. That is why the sheet thickness can be calculated along the direction of the sheet normal as a first estimate for the true wall thickness. The CPU cost for calculating the deep drawing forming operation of an aluminium alloy sheet using the TCCP-FE method amounts to only about eight times that for the Hill-based simulation. Due to this relatively slight difference in the total calculation time, it is possible to apply the TCCP-FE method for realistic forming simulations.

7. Conclusions

The texture component crystal plasticity FE method was used for simulating cup drawings of an aluminium alloy AlMg₃. The new simulation method accounts not only for the texture of the starting material but also for the texture development during forming. The integration of the method into commercial FEM software packages (MARC or ABAQUS) makes it easy to apply it to all kinds of starting microstructures, textures, and boundary conditions. It was shown that the prediction of the earing profile is in good agreement with the experimentally obtained earing profile. Some deviations of the simulated earing from the experimental result were attributed to insufficient approximation of the true textures by the texture component fit method. Moreover, the TCCP-FEM provides more exact results when compared to Hill's 1948 yield surface criterion, which does not account for the texture development during the forming simulation.

Acknowledgements

We gratefully acknowledge the kind financial support of the Deutsche Forschungsgemeinschaft (DFG, German Research

Foundation, www.dfg.de) which is funding this study within the Schwerpunktprogramm 1138 (modeling of scaling effects during processing).

References

- [1] D. Raabe, K. Helming, F. Roters, Z. Zhao, J. Hirsch, Texture component crystal plasticity finite element method for scalable large strain anisotropy simulations, in: Dong Nyung Lee (Ed.), Proceedings of the 13th International Conference on Textures of Materials ICOTOM 13, 2002, Seoul, Korea, Trans Tech Publications, Materials Science Forum, vols. 408–412, 2002, pp. 257–262.
- [2] F. Roters, H.S. Jeon-Haurand, D. Raabe, A texture evolution study using the texture component crystal plasticity FEM, in: Proceedings of the 14th International Conference on Textures of Materials ICOTOM 14, 2005, Leuven, Belgium, Materials Science Forum, vols. 495–497, 2005, pp. 937–944.
- [3] D. Raabe, F. Roters, Y. Wang, Simulation of earing during deep drawing of bcc steel by use of a texture component crystal plasticity finite element method, in: Proceedings of the 14th International Conference on Textures of Materials ICOTOM 14, 2005, Trans Tech Publications, Leuven, Belgium, Materials Science Forum, vols. 495–497, 2005, pp. 1529–1534.
- [4] Z. Zhao, F. Roters, W. Mao, D. Raabe, Introduction of a texture component crystal plasticity finite element method for industry-scale anisotropy simulations, *Adv. Eng. Mater.* 3 (2001) 984.
- [5] D. Raabe, P. Klose, B. Engl, K.-P. Imlau, F. Friedel, F. Roters, Concepts for integrating plastic anisotropy into metal forming simulations, *Adv. Eng. Mater.* 4 (2002) 169.
- [6] D. Raabe, F. Roters, Using texture components in crystal plasticity finite element simulations, *Int. J. Plast.* 20 (2004) 339.
- [7] Z. Zhao, W. Mao, F. Roters, D. Raabe, A texture optimization study for minimum earing in aluminium by use of a texture component crystal plasticity finite element method, *Acta Mater.* 52 (2004) 1003.
- [8] D. Raabe, Z. Zhao, F. Roters, Study on the orientational stability of cube-oriented FCC crystals under plane strain by use of a texture component crystal plasticity finite element method, *Scripta Mater.* 50 (2004) 1085.
- [9] D. Raabe, Y. Wang, F. Roters, Crystal plasticity simulation study on the influence of texture on earing in steel, *Comput. Mater. Sci.* 34 (2005) 221.
- [10] D. Raabe, Z. Zhao, F. Roters, A finite element method on the basis of texture components for fast predictions of anisotropic forming operations, *Steel Res.* 72 (2001) 421–426.
- [11] K. Lücke, J. Pospiech, J. Jura, J. Hirsch, On the presentation of orientation distribution functions by model functions, *Z. Metallkd.* 77 (1986) 312.
- [12] K. Helming, R.A. Schwarzer, B. Rauschenbach, S. Geier, B. Leiss, H. Wenk, K. Ullemeier, J. Heinitz, Texture estimates by means of components, *Z. Metallkd.* 85 (1994) 545.
- [13] D. Raabe, K. Lücke, Investigation of the ADC method for direct ODF approximation by means of standard functions, *Phys. Status Solidi (b)* 180 (1993) 59.
- [14] D. Raabe, K. Lücke, Analysis of the ADC method for direct ODF calculation by use of Gauss models and standard function, *Mater. Sci. Forum* 157–162 (1994) 413.
- [15] S. Kalidindi, C.A. Bronkhorst, L. Anand, Crystallographic texture evolution in bulk deformation processing of FCC metals, *J. Mech. Phys. Solids* 40 (1992) 537.
- [16] R. Hill, Theory of yield and plastic flow of anisotropic metals, *Proc. R. Soc. London A* 193 (1948) 281.
- [17] R. Hill, Theoretical plasticity of textured aggregates, *Math. Proc. Camb. Philos. Soc.* 85 (1979) 179.
- [18] W. Hosford, *The Mechanics of Crystals and Textured Polycrystals*, Oxford Univ. Press, 1993.
- [19] D. Banabic, O. Cazacu, F. Barlat, D.S. Comsa, S. Wagner, K. Siegert, Description of anisotropic behaviour of AA3103-0 aluminium alloy using two recent yield criteria, *Journal De Physique IV: JP 105* (2003) 297–304.
- [20] F. Barlat, J. Lian, Plastic behavior and stretchability of sheet metals. Part I: a yield function for orthotropic sheets under plane stress conditions, *Int. J. Plast.* 5 (1989) 51.

- [21] Theory and User Information, Version 2005, MSC Software Corporation, vol. A, Santa Ana, CA, USA, 2005, pp. 7–68.
- [22] D. Raabe, F. Roters, F. Barlat, L.-Q. Chen, (Herausgeber): Continuum Scale Simulation of Engineering Materials – Fundamentals – Microstructures – Process Applications, Wiley-VCH, Weinheim, June 2004, ISBN 3-527-30760-5.
- [23] H. Bunge, Texture Analysis in Materials Science, Butterworths, London, England, 1982.
- [24] P. Van Houtte, in: H.-R. Wenk (Ed.), Preferred Orientations in Deformed Metals and Rocks. An Introduction of Modern Texture Analysis, Academic Press, New York, 1985.
- [25] E. Aernoudt, P. Van Houtte, T. Leffers, Chapter 3, in: H. Mughrabi (Ed.), Deformation and Textures of Metals at Large Strain, vol. 6, in: R. W. Cahn, P. Haasen, E. J. Krämer (Eds.), Plastic Deformation and Fracture of Materials Science and Technology—A Comprehensive Treatment, VSH, Weinheim, 1993.
- [26] U. Kocks, C. Tóme, H. Wenk, Texture and Anisotropy, Cambridge University Press, 1998.
- [27] G. Wassermann, J. Grewen, Texturen Metallischer Werkstoffe, Springer-Verlag, Berlin, Germany, 1969 (in German).
- [28] A. Rollett, G. Canova, U. Kocks, in: A. K. Sachdev, J. D. Embury (Eds.), Proceedings of a TMS symposium on Metal Formability and Microstructure, TMS-AIME, Warrendale, 1986, p. 147.
- [29] J. Morris, Scripta Metall. Mater. 31 (1994) 387.
- [30] O. Daaland, E. Nes, Acta Mater. 44 (1996) 1389.
- [31] J. Savoie, Y. Zhou, J. Jonas, S. MacEwen, Acta Metall. 44 (1996) 587.
- [32] J. Hu, J. Jonas, T. Ishikawa, Mater. Sci. Eng. A256 (1998) 51.
- [33] X. Cheng, Y. Liu, J. Morris, Aluminum Trans. 1 (1999) 103.
- [34] K. Inal, P. Wu, K. Neale, Intern. J. Plast. 16 (2000) 635.
- [35] J. Yoon, F. Barlat, K. Chun, F. Pourboghra, D. Yang, Intern. J. Plast. 16 (2000) 1075.
- [36] X. Cheng, J. Morris, Mater. Sci. Eng. A 323 (2002) 32.
- [37] W. Liu, J. Morris, Through-thickness texture variation in cold-rolled AA 5182 aluminum alloy with an initial $\{001\}\langle 110 \rangle$ texture, Metall. Mater. Trans. A 36A (2005) 1329.
- [38] O. Engler, M.-Y. Huh, C. Tomé, A study of through-thickness texture gradients in rolled sheets, Metall. Mater. Trans. A 31A (2000) 2299.
- [39] J. Liu, S. Banovic, F. Biancianiello, R. Jiggetts, Through-thickness texture gradient in an annealed Al–Mg alloy sheet, Metall. Mater. Trans. A 36A (2005) 869.
- [40] H. Bunge, Mathematical Methods of Texture Analysis, Akademie Verlag, Berlin, 1969.
- [41] K. Helming, R. Schwarzer, B. Rauschenbach, S. Geier, B. Leiss, H. Wenk, K. Ullemeier, J. Heinitz, Z. Metallkd. 85 (1994) 545.
- [42] MSC, Marc user's manual, vol. D, MSC Software Corporation, 2001.
- [43] D. Raabe, M. Sachtleber, Z. Zhao, F. Roters, S. Zaefferer, Micromechanical and macromechanical effects in grain scale polycrystal plasticity experimentation and simulation, Acta Mater. 49 (2001) 3433–3441.
- [44] D. Raabe, Z. Zhao, S.-J. Park, F. Roters, Theory of orientation gradients in plastically strained crystals, Acta Mater. 50 (2002) 421–440.
- [45] M. Sachtleber, Z. Zhao, D. Raabe, Experimental investigation of plastic grain interaction, Mater. Sci. Eng. A 336 (2002) 81–87.
- [46] S. Zaefferer, J.-C. Kuo, Z. Zhao, M. Winning, D. Raabe, On the influence of the grain boundary misorientation on the plastic deformation of aluminum bicrystals, Acta Mater. 51 (2003) 4719–4735.
- [47] J.-C. Kuo, S. Zaefferer, Z. Zhao, M. Winning, D. Raabe, Deformation behaviour of aluminium-bicrystals, Adv. Eng. Mater. 5 (8) (2003) 563–566.